

Spatial Distributions of *Cryptosporidium* Oocysts in Porous Media: Evidence for Dual Mode Deposition

NATHALIE TUFENKJI*,† AND
MENACHEM ELIMELECH‡

Department of Chemical Engineering, McGill University, Montreal, Quebec H3A 2B2, Canada, and Department of Chemical Engineering, Environmental Engineering Program, Yale University, New Haven, Connecticut 06520-8286

Spatial distributions of *Cryptosporidium parvum* oocysts in columns packed with uniform glass-bead collectors were measured over a broad range of physicochemical conditions. Oocyst deposition behavior is shown to deviate from predictions based on classical colloid filtration theory (CFT) in the presence of repulsive (*unfavorable*) colloidal interactions. Specifically, CFT tends to predict greater removal of oocysts (less transport) than that observed in controlled laboratory experiments. Comparison of oocyst retention with results obtained using polystyrene latex particles of similar size suggests that mechanisms controlling particle deposition are the same in both systems. At a given ionic strength, the deposition of *Cryptosporidium* oocysts is generally greater than that of the microspheres; however, this discrepancy is partly attributable to large differences in oocyst and microsphere zeta potentials. A dual deposition mode (DDM) model is applied which considers the combined influence of “fast” and “slow” oocyst deposition due to the concurrent existence of *favorable* and *unfavorable* oocyst-collector interactions. Model simulations of retained oocyst profiles and suspended oocyst concentration at the column effluent are consistent with experimental data. Because classic CFT does not account for the effect of dual mode deposition (i.e., simultaneous “fast” and “slow” oocyst deposition), these observations have important implications for predictions of oocyst transport in subsurface environments, where repulsive electrostatic interactions predominate. Supporting elution experiments further suggest that specific surface interactions between oocyst wall macromolecules and the glass bead collectors could retard or even completely inhibit oocyst release upon perturbation in solution chemistry.

Introduction

Cryptosporidium parvum (*C. parvum*) has been identified as one of the most challenging microbial pathogens found in drinking water and is associated with a high risk of waterborne illness (1, 2). This protozoan parasite is transmitted via the fecal-oral route in its environmentally resistant stage—the

oocyst (1, 3, 4). Ingestion of a small number of viable oocysts (as little as 10) can lead to cryptosporidiosis, a diarrheal disease that is potentially lethal for immunosuppressed individuals (1, 2, 5, 6). Over the past two decades, several outbreaks of cryptosporidiosis related to both groundwater and surface water contamination have been reported in Europe and North America (3, 7, 8).

Resistance of the *C. parvum* oocyst to conventional disinfection processes (i.e., chlorination) poses a significant challenge to the protection of drinking water supplies from contamination (2, 9–11). As a result, water utilities are showing increased interest in oocyst removal in porous media, such as riverbank filtration, deep-bed (granular) filtration, and slow-sand filtration, to control drinking water quality (12–14). Moreover, there is a heightened interest in the use of surrogates to aid in monitoring pathogen transport in these environments, and thus comparison of oocyst removal with that of nonbiological particles is also useful. However, the mechanisms governing the transport and filtration behavior of *C. parvum* oocysts in these settings are not understood well enough to allow the development of predictive models for oocyst removal. For instance, a recent study showed that physical straining due to irregularity of grain shape plays an important role in the filtration of *C. parvum* oocysts in natural porous media (15). Yet, the influence of straining on particle removal is not considered in models commonly used to predict colloid transport in saturated porous media.

The transport and deposition behavior of colloidal particles in porous media—including microorganisms such as *C. parvum* oocysts—has traditionally been investigated using packed columns via measurements of the effluent fluid-phase particle concentration (16–28). Recent theoretical and experimental studies suggest that the shape of the retained profile of particles in column transport experiments can be a key indicator of particle removal mechanisms (29–31). In effect, researchers have examined the spatial distributions of retained microorganisms (e.g., bacteria and viruses) (32–37) in packed columns and shown that microbe deposition is generally inconsistent with classical colloid filtration theory (CFT)—the most commonly used approach for predicting particle deposition behavior in saturated porous media (38). Li et al. (39) broadened the scope of this issue by demonstrating deviation from CFT using nonbiological, latex colloids in the presence of repulsive electrostatic interactions. To further examine the validity of the classical CFT, Tufenkji and Elimelech (29, 31) conducted experiments using different-sized polystyrene latex particles in columns packed with spherical soda-lime glass beads over a broad range of physicochemical conditions. These studies revealed that in the presence of repulsive colloidal interactions (i.e., under conditions deemed *unfavorable* for deposition), secondary minimum deposition and particle retention on surface charge heterogeneities cause significant deviation from CFT (29, 31). Such investigations emphasize the importance of examining the profile of retained particles in column transport studies in an effort to better understand the mechanisms of particle removal in porous media (29–31, 39).

Although a number of studies have examined the spatial distributions of retained bacteria and viruses in packed-beds (32–37), such measurements are scarce in the literature regarding protozoan transport. Harter et al. (40) presented profiles of retained *C. parvum* oocysts in columns packed with natural sands and sediments. However, these experiments were conducted under relatively *favorable* conditions

* Corresponding author phone: (514)398-2999; fax: (514)398-6678; e-mail: nathalie.tufenkji@mcgill.ca.

† McGill University.

‡ Yale University.

for deposition, and therefore cannot be used to gain insight into the potential deviation from CFT in the presence of repulsive colloidal interactions. Mawdsley et al. (41) examined the distribution of *C. parvum* oocysts in columns packed with three different soil types, but these experiments were designed to simulate rainfall conditions and are therefore not consistent with classical CFT which is valid for saturated porous media only. Furthermore, in such physically and geochemically heterogeneous natural sediments, additional factors that are not accounted for in CFT may contribute to oocyst removal (e.g., physical straining, predation, and loss of viability) (41).

Deposition experiments carried out with *C. parvum* oocysts under well-controlled physicochemical conditions, in columns packed with uniform, spherical glass-bead collectors, can provide an improved mechanistic understanding of oocyst deposition. In particular, measurements of the spatial distribution of oocysts in the packed-bed can be used to verify how the deposition behavior of *C. parvum* deviates from predictions based on classical CFT. Tufenkji and Elimelech (31) recently demonstrated how spatial distributions of latex particles in packed columns are well described using a dual deposition mode (DDM) model which considers the combined influence of “fast” and “slow” particle deposition. Although the DDM model is in good agreement with measured concentrations of retained latex particles in columns packed with glass beads, this approach has not been tested with results of experiments involving microbes (e.g., *C. parvum* oocysts).

In this paper, we present well-controlled experiments with *C. parvum* oocysts and columns packed with spherical glass beads where we measure both the spatial distribution of retained oocysts and the suspended oocyst concentration over a broad range of physicochemical conditions. Comparison of oocyst retention with results obtained using similar-sized polystyrene latex particles suggests that the mechanisms controlling the observed deviation from CFT are the same in both systems. Furthermore, the validity of the DDM model in predicting the deposition behavior of *C. parvum* oocysts in porous media is assessed. Application of the DDM model suggests that the observed deviation from classical CFT is controlled by the combined influence of both “fast” and “slow” oocyst deposition; that is, a distribution in oocyst-collector interactions.

Materials and Methods

Porous Media. Spherical soda-lime glass beads (Class V, MO—SCI Corporation, Rolla, MO) were utilized as model collector grains. The manufacturer reported the average diameter of the glass beads as 0.328 mm. This grain size was selected to prevent possible straining of *C. parvum* oocysts during transport experiments (15). The glass beads are mainly composed of silica (70%) and other metal oxide impurities as reported previously (31). The glass beads were thoroughly cleaned to remove grease and other impurities as we described elsewhere (31).

Cryptosporidium Oocyst Source and Preparation. Viable oocysts were obtained from the Sterling Parasitology Laboratory (SPL) at the University of Arizona. The oocysts were shed from a calf infected with the Iowa isolate from Dr. Harley Moon (National Animal Disease Center, Ames, Iowa). Oocysts were purified (at SPL) using discontinuous sucrose and cesium chloride centrifugation gradients and stored (in the dark at 4 °C) in an antibiotic solution (0.01% Tween 20, 100U of penicillin, and 100 µg of gentamicin per mL). Before conducting experiments, oocysts were pelleted by centrifugation (12 000 rpm, 8050g for one minute), and the supernatant was replaced with 1 mL of deionized water (DI) (Nanopure Infinity, Barnstead Thermolyne Corporation,

Dubuque, IA). This step was repeated twice to remove any trace of the antibiotic solution. Purified oocysts were diluted to the desired concentration (2×10^6 oocysts/mL) in the electrolyte solution of interest prior to experiments.

Model Particles. Surfactant-free fluorescent polystyrene latex particles (EX 490 nm, EM 515 nm, Interfacial Dynamics Corporation, Portland, Oregon) with carboxyl-modified functional groups were used as model particles that can be compared to the oocyst deposition behavior. The monodispersed particles have a mean diameter of 3.0 µm and a density of 1.055 g/cm³, as described elsewhere (29, 31). These particles were selected to be of comparable size to the *C. parvum* oocysts.

Solution Chemistry. Analytical reagent-grade KCl (Fisher Scientific) and DI water were used to prepare electrolyte solutions. Salt concentrations were varied over a wide range of ionic strengths (1–300 mM) so that *favorable* and *unfavorable* deposition could be studied. The pH of the suspensions was adjusted to 8 by addition of KHCO₃ (1 mM).

Electrokinetic Characterization of Oocysts, Particles, and Collectors. Microelectrophoresis (ZetaPALS, Brookhaven Instruments Corporation, Holtsville, NY) was used to characterize the electrokinetic properties of the *C. parvum* oocysts and latex particles over the range of ionic strengths used in the column experiments. Electrophoretic mobility was measured at 25 °C (± 1 °C) using particle or oocyst suspensions (4.7×10^5 particles/mL) prepared in the background electrolyte of interest. Zeta potentials were calculated from the measured electrophoretic mobilities using the Smoluchowski equation (42). The electrokinetic properties of the glass beads were measured over the range of solution conditions used in the column experiments as described elsewhere (31).

Size Determination of Cryptosporidium Oocysts. The nominal size of the *C. parvum* oocysts was determined by analyzing images taken in an inverted fluorescent microscope operating in phase contrast mode at 63 × magnification (Axiovert 200m, Zeiss, Thornwood, NY). Ten microliters of an oocyst suspension (10^6 oocysts/mL at 30 mM ionic strength) was placed on a microscope slide and several images were recorded. Using an image processing program (ImageJ, NIH), the average diameter of the spherical oocysts was determined to be 4.3 ± 0.4 µm.

Deposition Experiments. Transport experiments were conducted by pumping a suspension of *C. parvum* oocysts or polystyrene latex particles through a glass chromatography column packed with clean soda-lime glass beads. An adjustable-height column (C 16/20, Amersham Biosciences, Piscataway, NJ) with an inner diameter of 1.6 cm was used. The soda-lime glass beads were wet-packed to a height of 12.6 cm with vibration to minimize any layering or air entrapment. Standard gravimetric methods were used to determine the glass bead density (2.43 g/cm³) and a column packing porosity of 0.37.

The packed column was equilibrated by pumping (Model 200 syringe pump, KD Scientific Inc., New Hope, PA) 20 pore volumes of the background electrolyte solution through the column at a constant approach (superficial) velocity of 8.3×10^{-3} cm/s. A suspension of *C. parvum* oocysts of the same background electrolyte composition was pumped for 2.8 pore volumes followed by an oocyst-free background electrolyte solution (2.8 pore volumes). A constant influent oocyst concentration (C_0) was maintained by including a miniature magnetic stir-bar in the oocyst solution syringe. Similar deposition experiments were also conducted using latex particles of comparable size to the *C. parvum* oocysts. Particle concentration at the column outlet was monitored on-line using optical density measurements (at 330 and 360 nm for *C. parvum* oocysts and latex particles, respectively) with a UV/visible spectrophotometer (Hewlett-Packard Model 8453)

and a 1 cm flow-through cell. The influent oocyst concentration was maintained constant in all experiments ($C_0 = 2 \times 10^6$ oocysts/mL). This oocyst concentration corresponds to an absorbance of 0.32 at 360 nm. To obtain optimal resolution, the influent concentration of latex particles was varied between experiments, namely, $C_0 = 1.7 \times 10^7$ particles/mL for experiments at lower ionic strengths (3, 10, 30 mM) and $C_0 = 5.4 \times 10^6$ particles/mL for experiments conducted at higher ionic strengths (100, 300 mM). The total amount of retained particles (N_{dep}) was determined by calculating the difference between the number of particles injected into the column (N_{inj}) and the amount obtained by numerically integrating the particle breakthrough curve (N_{eff}).

In a few experiments, two additional pulses of particle-free electrolyte solutions were pumped through the column to initiate the elution (release) of previously deposited *C. parvum* oocysts or latex particles. A pulse of low ionic strength solution (0.1 mM KHCO_3) was first pumped through the column, followed by an injection of a pH 11 solution (1 mM KOH). The total number of oocysts or latex particles released (N_{rel}) was calculated by numerically integrating the two elution pulses, to determine the fraction of released oocysts or latex particles, f_{rel} , where $f_{rel} = N_{rel}/N_{dep}$.

Column Dissection and Enumeration of Retained Oocysts and Particles. After completing an oocyst deposition experiment, the packed bed was dissected into sections to obtain the spatial distribution of *C. parvum* oocysts in the column. The bottom end-piece was removed without disturbing the packed bed, and the porous medium was extruded in 1-cm wide sections by gravity. The packed bed remained saturated with electrolyte solution during the entire extrusion process so as not to shift or cause release of retained oocysts. This procedure was also carried out for column deposition experiments conducted with polystyrene latex particles.

Retained oocyst and latex particle concentrations in each packed-bed section were determined using a fluorescent microscope as described elsewhere (31). In experiments conducted with *C. parvum*, oocysts were stained with FITC (fluorescein isothiocyanate) monoclonal antibody (Meridian Scientific, Cincinnati, OH) prior to counting in the fluorescent microscope. At the conclusion of each experiment, the soda-lime glass beads were discarded.

In each experiment, the mass balance of *C. parvum* oocysts or latex particles was determined by comparing the number of deposited particles calculated from integrating the particle breakthrough curve (N_{dep}) to the amount retained based on enumeration in the fluorescent microscope. In general, the mass balance was within $\pm 15\%$, but in most experiments the mass balance was $\pm 9\%$.

Calculation of Attachment (Collision) Efficiency. In classical colloid filtration theory (CFT), particle removal is represented by first-order kinetics, resulting in concentrations of suspended $C(x)$ and retained particles $S(x)$ that decay exponentially with distance

$$C(x) = C_0 \exp\left[-\frac{k}{v}x\right] \quad (1)$$

$$S(x) = \frac{t_0 \epsilon k}{\rho_b} C(x) = \frac{t_0 \epsilon k C_0}{\rho_b} \exp\left[-\frac{k}{v}x\right] \quad (2)$$

where k is the particle deposition rate coefficient, v is the interstitial particle velocity, ϵ is the bed porosity, ρ_b is the porous medium bulk density, and t_0 is the duration of continuous particle injection at concentration C_0 (at $x = 0$). The particle deposition rate coefficient, k , is related to the commonly used single-collector removal efficiency η as described elsewhere (30, 31).

Particle attachment (collision) efficiencies, α , were calculated for experiments conducted with *C. parvum* oocysts

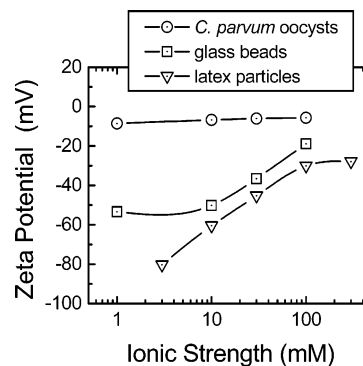


FIGURE 1. Zeta (ζ) potentials of (○) *C. parvum* oocysts, (▽) 3.0 μm polystyrene latex particles, and (□) soda-lime glass beads over a range of ionic strengths (KCl) at pH 8 (1 mM KHCO_3).

and latex particles at different solution ionic strengths (38, 43). The attachment efficiency is defined as the ratio of the experimental single-collector removal efficiency (η) and the predicted single-collector contact efficiency (η_0) evaluated from solution of the convective-diffusion equation in the absence of repulsive interaction energies, i.e., $\alpha = \eta/\eta_0$ (24, 38, 44). The value of η_0 for the described experimental conditions was calculated using a new correlation equation based on a rigorous numerical solution of the convective-diffusion equation (44)

$$\eta_0 = 2.4A_S^{1/3} N_R^{-0.081} N_{Pe}^{-0.715} N_{vdW}^{0.052} + 0.55A_S N_R^{1.675} N_A^{0.125} + 0.22N_R^{-0.24} N_G^{1.11} N_{vdW}^{0.053} \quad (3)$$

where N_R is an aspect ratio, N_{Pe} is the Peclet number, N_A is the attraction number, N_{vdW} is the van der Waals number, and N_G is the gravity number.

The value of the attachment efficiency can be calculated from the particle breakthrough curve (α_{BTC}) using eq 1 and the normalized column effluent concentration $C/C_{0|x=L}$ at the initial stages of deposition (31). In addition, linearization of eq 2 reveals that the particle deposition rate coefficient, k , and thus the attachment efficiency, α , can be obtained from the slope (α_{SLOPE}) of a semilog plot of the retained particle profile, $S(x)$ (31).

Results and Discussion

Electrokinetic Properties of Oocysts, Particles, and Collectors. The zeta (ζ) potentials of the *C. parvum* oocysts, polystyrene latex particles, and soda-lime glass beads as a function of ionic strength are presented in Figure 1. The *C. parvum* oocysts, latex particles, and glass beads are negatively charged at the solution conditions investigated (pH 8), and their zeta potentials become less negative with increasing ionic strength. It is interesting to note that the zeta potential of the *C. parvum* oocysts is low (~ -6 mV) in comparison to that of the latex particles ($-80 < \zeta < -30$) and remains nearly constant over the range of ionic strengths investigated. This was also reported previously by Dai and Hozalski (45) and Brush et al. (46). The oocysts used here were obtained from the same source as a previous study; however, in the latter case, oocysts were heat-inactivated (15). Under similar solution conditions, Tufenkji et al. (15) observed much more negative zeta potentials. Such variation in oocyst ζ with changes in oocyst pretreatment methods has previously been reported (46, 47). Measured zeta potentials are used later to calculate Derjaguin-Landau-Verwey-Overbeek (DLVO) interaction energy profiles for the oocyst-glass bead system and the latex-glass bead system.

Transport and Deposition Kinetics of Oocysts and Latex Microspheres. Oocyst and latex microsphere breakthrough curves obtained at different solution ionic strengths are

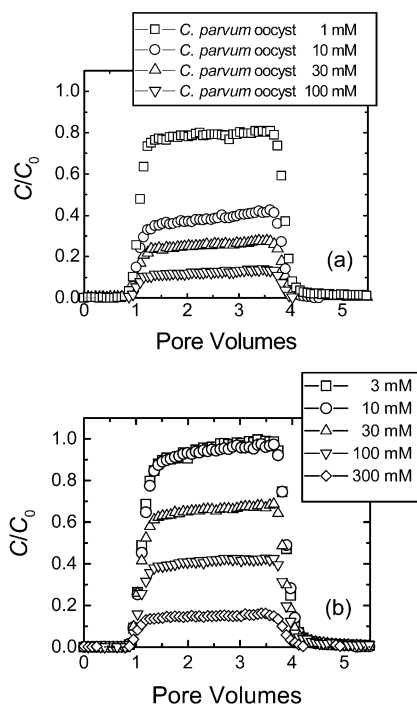


FIGURE 2. Representative breakthrough curves for experiments conducted with (a) *C. parvum* oocysts and (b) 3.0 μm latex particles in columns packed with soda-lime glass beads over a wide range of solution ionic strengths. Key experimental conditions were as follows: approach velocity = 8.3×10^{-3} cm/s, porosity = 0.37, mean bead diameter = 0.328 mm, pH = 8.0–8.3, and temperature = 20–22 °C.

presented in parts a and b, respectively, of Figure 2. Here, the normalized effluent oocyst or microsphere concentration (C/C_0) is plotted as a function of pore volumes. The deposition of *C. parvum* oocysts and latex particles on the glass beads increases (C/C_0 decreases) with increasing ionic strength, in qualitative agreement with the DLVO theory of colloidal stability (48, 49). As the concentration of KCl in the background electrolyte solution increases, the repulsive electrostatic double-layer forces are lessened resulting in increased particle deposition rates.

The experimental results presented in Figure 2 can be compared quantitatively by calculating the attachment efficiency, α_{BTC} , from the normalized effluent particle concentration (C/C_0) in each particle breakthrough curve and the value of η_0 determined from eq 3 ($\alpha = \eta/\eta_0$). In absence of literature values for the Hamaker constant of the glass-water-oocyst system, a value of 6.5×10^{-21} J—similar to that reported for interaction of bacterial cells with quartz in an aqueous medium (50)—was used to calculate the single-collector contact efficiency for *C. parvum* oocysts ($\eta_{0,oocyst} = 1.1 \times 10^{-2}$). An oocyst density of 1047 kg/m³ was used in this calculation (51). In determining the single-collector contact efficiency for latex microspheres ($\eta_{0,microsphere} = 7.9 \times 10^{-3}$), the value of the Hamaker constant for the glass-water-polystyrene system was taken as 1×10^{-20} J (24, 25, 52).

Attachment efficiencies calculated from both oocyst and microsphere breakthrough curves are presented in Table 1 as a function of solution ionic strength (with other parameters to be discussed later). As mentioned earlier, the observed deposition behavior follows the trend predicted by DLVO theory. An increase in salt concentration from 1 to 100 mM yields an increase in α_{BTC} for the *C. parvum* oocysts from 0.063 to 0.55. Similarly, values of α_{BTC} for the latex microspheres increase from 0.019 to 0.68 with an increase in ionic strength from 3 to 300 mM.

TABLE 1. Experimentally Determined Oocyst and Microsphere Attachment Efficiencies and Calculated DLVO Parameters

ionic strength (mM)	attachment efficiency, α_{BTC}		<i>C. parvum</i> oocyst		latex microsphere	
	<i>C. parvum</i> oocyst ^a	latex microsphere ^b	Φ_{max} ($k_B T$)	$\Phi_{2^{min}}$ ($k_B T$)	Φ_{max} ($k_B T$)	$\Phi_{2^{min}}$ ($k_B T$)
1	0.063	NM ^c	320	0.33	ND ^d	ND ^d
3	NM ^c	0.019	ND ^d	ND ^d	7500	0.85
10	0.26	0.032	130	5.5	4800	3.6
30	0.37	0.13	1.2	24	1900	14
100	0.55	0.31	NB ^e	NB ^e	12	72
300	NM ^c	0.68	ND ^d	ND ^d	NB ^e	NB ^e

^a The value of the single-collector contact efficiency for *C. parvum* oocysts ($\eta_0 = 1.1 \times 10^{-2}$) was calculated using eq 3 and the following parameter values: $d_p = 4.3 \mu\text{m}$, $d_c = 328 \mu\text{m}$, $U = 8.3 \times 10^{-5}$ m/s, $A = 6.5 \times 10^{-21}$ J, $T = 293$ K, $\rho_p = 1047$ kg/m³, $\rho_f = 1000$ kg/m³, $\mu = 1.005 \times 10^{-3}$ kg/m s, $\epsilon = 0.37$. ^b The value of the single-collector contact efficiency for latex microspheres ($\eta_0 = 7.9 \times 10^{-3}$) was calculated as indicated above except for the following: $d_p = 3.0 \mu\text{m}$, $A = 1 \times 10^{-20}$ J, and $\rho_p = 1055$ kg/m³. ^c Not measured (i.e., column experiment not conducted under given condition). ^d Not determined. ^e No calculated barrier to deposition and, hence, no predicted secondary minimum.

The results in Table 1 emphasize the variation in deposition rates observed for *C. parvum* oocysts in comparison to latex microspheres under identical solution conditions. For instance, at 10 mM the value of α_{BTC} for the oocysts is 0.26, whereas for the microspheres it is only 0.032. This large discrepancy in measured attachment efficiencies can be partly attributed to the observed differences in oocyst and microsphere zeta potentials (Figure 1). Variations in particle zeta potentials will be reflected in the total interaction energy profiles for the oocyst-glass bead system and the latex-glass bead system.

DLVO Interaction Energy Calculations. To better understand the variation in the observed degree of oocyst and microsphere retention, DLVO theory is used to calculate colloidal interaction energies. DLVO theory considers the sum of London-van der Waals (VDW) attraction and electrostatic double-layer (EDL) repulsion. The total interaction energy, namely, the sum of VDW and EDL interactions, was determined by treating the oocyst-glass bead system and the microsphere-glass bead system as sphere-plate interactions. EDL interactions were calculated from the expression of Hogg et al. (53) for interaction at a constant surface potential, with the zeta potentials of the *C. parvum* oocysts, latex particles, and soda-lime glass beads being used in place of the respective surface potentials. The VDW attractive energy was calculated from the expression proposed by Gregory (54) for retarded VDW interaction. A value of 1×10^{-20} J was chosen for the Hamaker constant of the polystyrene-water-glass system (24, 25, 52), whereas a value of 6.5×10^{-21} J was used for the oocyst-water-glass system (50).

Key parameters determined from DLVO interaction energy profiles for the oocyst-glass bead system and the microsphere-glass bead system are presented in Table 1 as a function of solution ionic strength. The calculations reveal the presence of a significant repulsive energy barrier to deposition (Φ_{max}) for the latex particles at nearly all ionic strengths, ranging from 7500 $k_B T$ at 3 mM to 12 $k_B T$ at 100 mM. In contrast, much lower energy barriers to deposition are predicted for the oocyst-glass bead system, ranging from 320 $k_B T$ at 1 mM to 1.2 $k_B T$ at 30 mM. To some extent, this variation in the energy barrier predicted by DLVO theory can account for the significant differences in measured oocyst and microsphere attachment efficiencies. For instance, at 10 mM, where the value of α_{BTC} for the oocysts is 0.26 and that for the microspheres is 0.032, the energy barrier for the oocyst-glass bead system ($\Phi_{max} = 130 k_B T$) is considerably lower

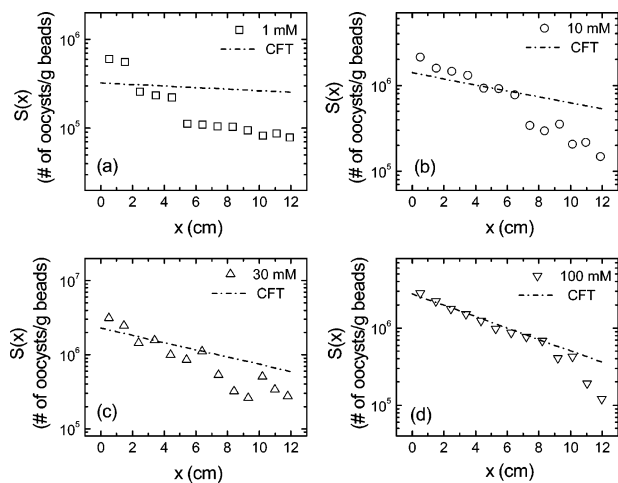


FIGURE 3. Comparison of experimental retained *C. parvum* oocyst concentration profiles (symbols) and predictions based on classical CFT using α_{BTC} determined from the corresponding breakthrough curve (dashed lines) for different solution ionic strengths: (a) 1 mM, (b) 10 mM, (c) 30 mM, and (d) 100 mM. Experimental conditions were the same as in Figure 2a.

than that predicted for the latex-glass bead system ($\Phi_{max} = 4800 k_B T$).

Also shown in Table 1 are the depths of the secondary energy minimum ($\Phi_{2^o_{min}}$) predicted for the oocyst-glass bead interaction and the microsphere-glass bead interaction as a function of ionic strength. A secondary energy well exists because the EDL interaction decreases exponentially with respect to separation distance, whereas the VDW attraction exhibits a slower power-law decay. DLVO theory predicts an increase in the depth of the secondary energy well with increasing ionic strength, particle size, and Hamaker constant of the interacting media. These calculations indicate that the magnitudes of $\Phi_{2^o_{min}}$ for the oocyst-glass bead system and the microsphere-glass bead system are comparable. For instance, at 10 mM, the value of $\Phi_{2^o_{min}}$ for the oocyst-glass bead interaction is $5.5 k_B T$, whereas for the latex-glass bead interaction, it is $3.6 k_B T$.

It has been proposed that the observed attachment of colloidal particles in the presence of a relatively high energy barrier (as predicted here for oocysts and microspheres at the lower ionic strengths) can be partially attributed to deposition in the secondary energy well (27, 31, 55, 56). The relatively deep energy wells predicted here for both systems suggest that particles could readily be retained, even at the low ionic strengths considered. This concept will be examined in more detail later in the paper.

Spatial Distributions of Oocysts and Microspheres in Packed Beds. It has been shown that the shape of the retained profile of particles following a typical column experiment can be a key indicator of the mechanisms controlling particle transport and deposition (30, 31). However, as described earlier, well-controlled column studies conducted with *C. parvum* oocysts, where the spatial distribution of retained oocysts has been quantified over a wide range of physico-chemical conditions, are virtually nonexistent. Here, we present spatial distributions of retained *C. parvum* oocysts or microspheres obtained by carefully dissecting the packed-bed following the completion of each deposition experiment. In Figure 3, the profiles of retained oocysts corresponding to the breakthrough curves in Figure 2a are shown. Similarly, in Figure 4, the profiles of retained latex microspheres corresponding to the breakthrough curves in Figure 2b are shown. In these graphs, the retained particle concentration, $S(x)$, is plotted as a function of distance in a semilog format. Included in each figure for comparison are the spatial

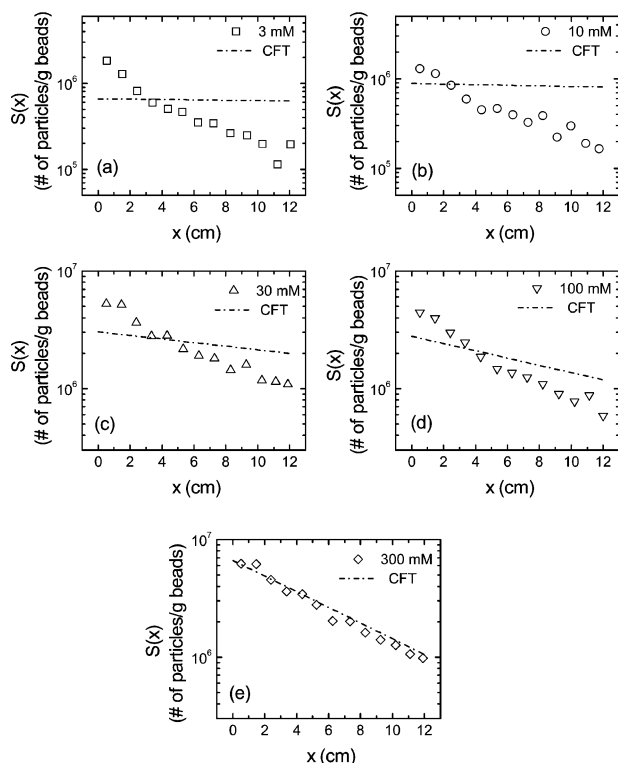


FIGURE 4. Comparison of experimental retained latex microsphere concentration profiles (symbols) and predictions based on classical CFT using α_{BTC} determined from the corresponding breakthrough curve (dashed lines) for different solution ionic strengths: (a) 3 mM, (b) 10 mM, (c) 30 mM, (d) 100 mM, and (e) 300 mM. Experimental conditions were the same as in Figure 2b.

distributions of oocysts or latex microspheres predicted by CFT (eq 2) using the attachment efficiency determined from the corresponding breakthrough curve (α_{BTC}).

Inspection of Figures 3 and 4 reveals that the measured concentrations of *C. parvum* oocysts and microspheres are generally in marked disagreement with those predicted by classical CFT, with the exception of those measured at the higher ionic strengths (100 mM and 300 mM, for the oocysts and microspheres, respectively). This observed behavior is consistent with previously reported findings using model colloidal particles and bacteria (31, 36, 39). It is interesting to note that with increasing ionic strength, the measured spatial distribution of *C. parvum* oocysts and latex microspheres approaches that calculated using values of α_{BTC} (i.e., that predicted by CFT).

Comparison of Oocyst and Latex Microsphere Attachment Efficiencies. To compare the differing degrees of deviation from CFT obtained with *C. parvum* oocysts and latex particles, the value of the attachment efficiency, α_{SLOPE} , was calculated from the slope of each profile of retained particles, $S(x)$, and compared with attachment efficiencies calculated from the corresponding breakthrough curves, α_{BTC} (Figure 5). In such a plot, data points falling on the dashed line (slope of 1 and intercept of zero) indicate perfect agreement between values of the attachment efficiency calculated from the oocyst or microsphere breakthrough curve (α_{BTC}) and the attachment efficiency determined from the slope of the corresponding retained profile (α_{SLOPE}).

Inspection of Figure 5 reveals that the behavior of *C. parvum* oocysts in columns packed with glass beads is nearly identical to that observed with latex microspheres of comparable size. The data points measured from the breakthrough curves and retained profiles obtained with *C. parvum* oocysts fall in the same region of the plot as the

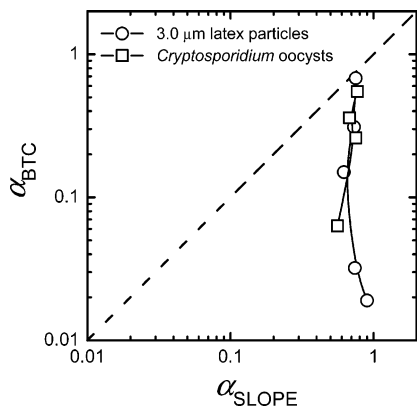


FIGURE 5. Comparison of attachment efficiencies determined from the slope of retained particle profiles (α_{SLOPE}) and attachment efficiencies calculated from particle breakthrough curves (α_{BTC}) for (\square) *C. parvum* oocysts and (\circ) $3\ \mu\text{m}$ latex particles. Experimental conditions were the same as in Figure 2 and are summarized in Table 1.

values measured from the experiments conducted with latex microspheres. At the higher ionic strengths considered (100 and 300 mM, for the oocysts and latex particles, respectively), calculated values of α_{SLOPE} are nearly identical to corresponding values of α_{BTC} (i.e., data points are very close to the dashed line). As the salt concentration in solution decreases (i.e., decreasing values of α_{BTC} on the vertical axis), the deviation between values of α_{SLOPE} and α_{BTC} increases considerably and in a comparable manner for both oocysts and latex microspheres.

Using well-controlled experiments with polystyrene latex particles, Tufenkji and Elimelech (29, 31) have recently shown that the observed deviation from CFT in the presence of repulsive electrostatic interactions can be largely attributed to the concurrent existence of both *favorable* and *unfavorable* particle-collector interactions. In particular, the results demonstrate that both secondary minimum deposition and surface charge heterogeneities contribute significantly to the deviation from CFT generally observed in colloid transport studies. Tufenkji and Elimelech (29, 31) propose that under conditions generally considered *unfavorable* for deposition (i.e., in the presence of a predicted repulsive energy barrier), the occurrence of a relatively deep secondary energy well or chemical heterogeneities in the form of near-neutrally or positively charged regions of particle and/or collector surfaces can give rise to local *favorable* deposition conditions. In theory, particles or oocysts that deposit in the primary energy well after overcoming the energy barrier will exhibit a relatively “slow” or hindered rate of deposition. Thus, in this case, the occurrence of local *favorable* conditions for deposition will give rise to a distributed particle or oocyst population (29, 31). The results shown in Figure 5, where the data points measured using *C. parvum* oocysts are in good agreement with those measured using latex microspheres, suggest that the proposed mechanisms causing deviation from CFT for latex particles in columns packed with clean glass bead collectors are the same as those controlling the behavior of the *C. parvum* oocysts.

The agreement in the two data sets depicted in Figure 5 can be partially rationalized by considering the mechanisms proposed by Tufenkji and Elimelech (29, 31) as well as calculated DLVO parameters presented in Table 1. As described previously, both the oocyst-glass bead system and the microsphere-glass bead system exhibit relatively deep secondary energy wells over the range of ionic strengths investigated (Table 1). In addition, the influence of charge heterogeneities on the collector surface should be comparable in both systems since similar clean glass-beads were used.

Thus, both secondary minimum deposition and particle retention on surface charge heterogeneities are expected to contribute to the deviation from CFT observed in the two experimental systems.

Dual Deposition Mode Can Explain Oocyst Deposition Behavior. In the presence of repulsive DLVO interactions, particles may exhibit a dual deposition mode whereby a fraction of the particle population experiences a “fast” deposition rate and the remaining particles deposit at a “slow” rate (29, 31). For instance, the presence of a deep secondary energy minimum as well as charge heterogeneities on particle and/or collector surfaces can provide conditions for *favorable* or “fast” particle deposition, where the attachment efficiency, α , approaches unity. In contrast, the general occurrence of repulsive energy barriers (*unfavorable* condition) gives rise to particle deposition rates which are much “slower”, characterized by lower values of the attachment efficiency, i.e., $\alpha \ll 1$.

The concurrent existence of both *favorable* and *unfavorable* conditions in an otherwise homogeneous system can be described by including a bimodal distribution of k in the classical colloid filtration theory (30, 31)

$$C(x) = C_0 \int_0^\infty \exp\left[-\frac{k}{v}x\right] p(k) dk \quad (4)$$

$$S(x) = \frac{\epsilon t_0 C_0}{\rho_b} \int_0^\infty k \exp\left[-\frac{k}{v}x\right] p(k) dk \quad (5)$$

where $C(x)$ is the suspended particle concentration, $S(x)$ is the retained particle concentration, and $p(k)$ is the linear combination of two normal (Gaussian) distributions:

$$p(k) = f_{\text{slow}} \frac{1}{\sigma_{\text{slow}} \sqrt{2\pi}} \exp\left[-\frac{1}{2} \left(\frac{k - \bar{k}_{\text{slow}}}{\sigma_{\text{slow}}}\right)^2\right] + f_{\text{fast}} \frac{1}{\sigma_{\text{fast}} \sqrt{2\pi}} \exp\left[-\frac{1}{2} \left(\frac{k - \bar{k}_{\text{fast}}}{\sigma_{\text{fast}}}\right)^2\right] \quad (6)$$

Here, \bar{k}_{slow} and \bar{k}_{fast} are the mean deposition rate coefficients, σ_{slow} and σ_{fast} are the corresponding standard deviations, and f_{slow} and f_{fast} are the fractions of the total population associated with each mode. This Dual Deposition Mode (DDM) model (eqs 4–6) has successfully been applied to describe the deposition behavior of latex particles in columns packed with glass beads over a broad range of solution conditions (31).

In Figure 6, profiles of retained *C. parvum* oocysts measured at different solution ionic strengths (open symbols) are compared to calculations based on the proposed DDM model (solid lines) as well as classical CFT (dashed lines). Equations 5 and 6 were fit to the measured spatial distribution of oocysts by nonlinear regression using a Levenberg–Marquardt approach. The two parameters varied during the optimization procedure are the mean deposition rate coefficient \bar{k}_{slow} and the fraction f_{slow} of the total population associated with this mode. The mean deposition rate coefficient of the rapidly depositing fraction \bar{k}_{fast} was determined by setting the maximum deposition rate coefficient k_{max} equal to the transport limited rate (i.e., $\alpha_{\text{max}} = 1$), where $k_{\text{max}} = \bar{k}_{\text{fast}} + 3\sigma_{\text{fast}}$ (31). Because this mode of the distribution takes into account the deposition of oocysts under *favorable* conditions (i.e., those retained in the secondary energy well or on surface charge heterogeneities), it follows that the maximum value of the attachment efficiency should equal 1. For such conditions, the distribution in the oocyst deposition rate coefficient is considered to be relatively narrow; thus, the standard deviation associated to this mode (σ_{fast}) was calculated as 5% of the mean, \bar{k}_{fast} . When k_{max} is equal to the transport limited rate and $\sigma_{\text{fast}} = 0.05 \bar{k}_{\text{fast}}$, then the mean attachment efficiency α_{fast} is determined to be 0.87.

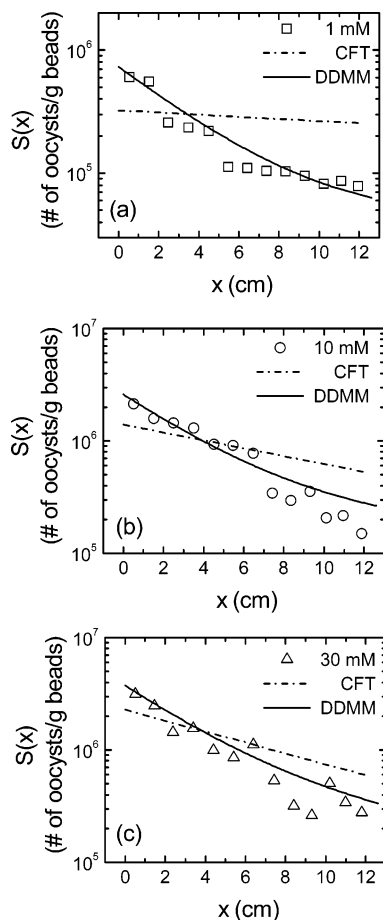


FIGURE 6. Comparison of experimental retained particle concentration profiles (symbols) and predictions based on the proposed DDM model with two fitting parameters (solid lines) and the classical CFT using α_{BTC} determined from the corresponding breakthrough curve (dashed lines) for different solution ionic strengths: (a) 1 mM, (b) 10 mM, and (c) 30 mM. Experimental conditions were the same as in Figure 2. Fitted DDM model parameters were the mean deposition rate coefficient \bar{k}_{slow} and the fraction f_{slow} of the total population associated with this mode. Model parameters and predictions are summarized in Table 2.

For the case where oocysts need to overcome an energy barrier to deposit in the primary energy well (i.e., “slow” deposition), a wider distribution in k is considered; thus, σ_{slow} was set equal to 15% of \bar{k}_{slow} . It should be noted that the resulting model fits and parameter values were not very sensitive to the values of these standard deviations. Indeed, DDM model fits and parameter values were nearly identical when the coefficient of variation ($CV = \sigma/\bar{k}$) was increased to as much as 30% or decreased to nil. This suggests that a *discrete* bimodal distribution in particle deposition rates could also be used to effectively describe the observed particle or microbe deposition behavior (e.g., ref 33). Such an approach would be simpler to implement.

The comparison shown in Figure 6 indicates that the DDM model adequately captures the deposition behavior of the *C. parvum* oocysts over the range of solution conditions investigated, even when only two model parameters are varied. Other studies have used a similar modeling approach to describe observed spatial distributions of retained microorganisms, where a distribution in microbial deposition rates was considered (33, 57). However, in these investigations, three fitting parameters were required to optimize model predictions. The proposed DDM model is consistent with the observed oocyst deposition behavior, as demonstrated by calculated values of the adjusted coefficient of

TABLE 2. Comparison of Calculated Dual Deposition Mode (DDM) Model Parameters and Experimental Results for Oocyst Deposition

ionic strength (mM)	DDM model parameters and predictions					experimental results	
	$\bar{\alpha}_{fast}^a$	$\bar{\alpha}_{slow}^b$	f_{fast}^b	$C/C_0 _{x=L}^c$	R_{adj}^2	$C/C_0 _{x=L}^d$	f_{rel}^e
1	0.87	0.010	0.15	0.82	0.90	0.78	NM ^f
10	0.87	0.10	0.47	0.38	0.94	0.36	NM ^f
30	0.87	0.17	0.57	0.25	0.90	0.23	0.23

^a Calculated from $\alpha_{max} = 1$, where $\alpha_{max} = \bar{\alpha}_{fast} + 3(0.05)\bar{\alpha}_{fast}$.
^b Determined by nonlinear regression of eq 5 to measured profile of retained oocysts. Note: $f_{fast} = 1 - f_{slow}$.
^c Predicted by DDM model (eq 4).
^d Determined by averaging over pore volumes 1.8–2.
^e Determined by integration of elution peaks in Figure 7a.
^f Not measured.

determination (R_{adj}^2) which are presented in Table 2 (with other parameters to be discussed later).

Values of model parameters (reported as $\bar{\alpha}_{slow}$ and f_{fast}) determined for the *C. parvum* experiments conducted at 1, 10, and 30 mM are shown in Table 2. Observed trends in the values of these parameters with changing solution ionic strength correspond to those noted previously for experiments conducted with similarly sized latex microspheres (31). For instance, inspection of Table 2 reveals that fitted values of $\bar{\alpha}_{slow}$ become larger with increasing ionic strength, from 0.01 at 1 mM to 0.17 at 30 mM. This behavior can be attributed to an increase in the efficiency of oocysts in overcoming the repulsive energy barrier as the height of this barrier diminishes with increasing ionic strength. The fraction of the oocyst population that experiences a “fast” deposition rate, f_{fast} , (where $f_{fast} = 1 - f_{slow}$) also increases with solution salt concentration. As solution ionic strength increases, the extent of *favorable* deposition conditions becomes more significant (i.e., there is a higher probability of oocysts encountering a deep secondary energy well and/or a near-neutrally charged surface heterogeneity).

Also included in Table 2 are predicted and measured values of the normalized column effluent concentration, $C/C_0|_{x=L}$, as a function of solution ionic strength. Predictions of $C/C_0|_{x=L}$ were obtained using eqs 4 and 6 with the optimized and calculated model parameters. Results predicted by the DDM model are in good agreement with measurements of $C/C_0|_{x=L}$ over the range of ionic strengths investigated.

Supporting Evidence for Dual Mode Deposition of *Cryptosporidium* Oocysts. Experimental validation of model fitting parameters is a considerable challenge in applying transport models to describe observed particle deposition behavior. As mentioned earlier, the DDM model has been successfully applied to describe the deposition behavior of latex microspheres over a wide range of solution ionic strengths (31). In this study, optimized DDM model parameters were verified experimentally using elution experiments, where the fraction of particles eluted following injection of low ionic strength and high pH solutions was quantified (31). It has been proposed that the elution of deposited particles following exposure to a low ionic strength solution can be attributed to release from the secondary energy minimum (20, 21, 27, 55, 56, 58). Likewise, an injection of a high pH solution should promote release of particles retained on surface charge heterogeneities such as metal oxide impurities (59). Thus, an elution experiment, where retained particles are exposed to a series of particle-free electrolyte solutions, should provide insight into the mechanisms controlling particle deposition.

In the elution experiments carried out in this study, two additional pulses of particle-free solutions were pumped through the column following a typical particle injection: (i) a pulse of much lower ionic strength (0.1 mM $KHCO_3$) to

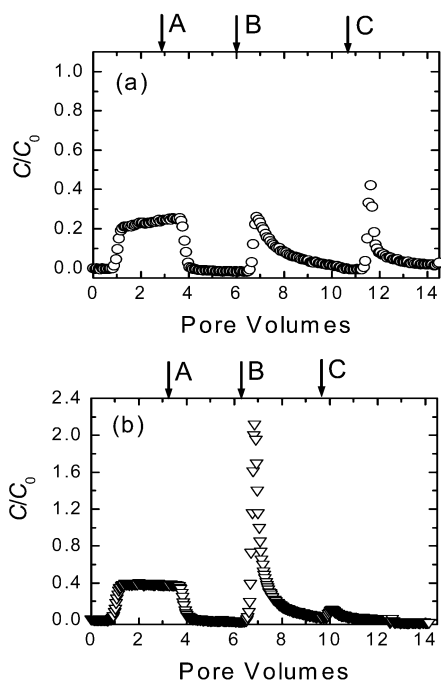


FIGURE 7. Representative breakthrough curves for elution experiments conducted with (a) *C. parvum* oocysts at 30 mM and (b) latex microspheres at 100 mM. Arrows indicate the injection of (A) a particle-free solution at the same ionic strength as the deposition phase (pH 8); (B) a particle-free solution at low ionic strength (0.1 mM KHCO_3); and (C) a particle-free solution at low ionic strength and high pH (1 mM KOH, pH 11). Other experimental conditions were the same as in Figure 2.

eliminate the presence of the secondary minimum and (ii) a solution at pH 11 (1 mM KOH) to promote release of particles deposited on surface charge heterogeneities. Breakthrough curves for elution experiments conducted with *C. parvum* oocysts (at 30 mM) and similarly sized latex microspheres (at 100 mM) are shown in parts a and b, respectively, of Figure 7. These two experiments were selected for comparison because they exhibit comparable degrees of particle removal (i.e., the value of α_{BTC} for *C. parvum* oocysts at 30 mM is 0.38, whereas for latex colloids at 100 mM, $\alpha_{\text{BTC}} = 0.33$).

The fraction of released oocysts, f_{rel} , was calculated by numerically integrating the two elution pulses in Figure 7a (N_{rel}) and dividing by the total number of oocysts deposited during the first phase of the experiment (N_{dep}) (Table 2, rightmost column). In a similar investigation conducted with uniform latex particles, Tufenkji and Elimelech (31) showed that the fraction of particles released following injection of low ionic strength and high pH solutions was in excellent agreement with values of the fitted DDM model parameter, f_{fast} . For instance, when particles were deposited at 100 mM ionic strength (Figure 7b), the measured fraction of particles released, f_{rel} , was 0.62 whereas the fitted DDM model parameter, f_{fast} , was 0.61. However, in the experiment conducted here with *C. parvum* oocysts (Figure 7a), the measured value of f_{rel} is not very close to the optimized DDM model parameter value (i.e., $f_{\text{rel}} = 0.23$ whereas $f_{\text{fast}} = 0.57$). If secondary minimum deposition and retention on surface charge heterogeneities were the key mechanisms controlling oocyst deposition (as suggested by the experiments conducted with model particles (31)), then the fraction of oocysts eluted should correspond to the fraction of oocysts that deposit at a “fast” rate. Yet, the measured value of f_{rel} is nearly one-third that of the fitted model parameter, f_{fast} .

This discrepancy in values of f_{rel} and f_{fast} for the *C. parvum* elution experiment may be attributed to specific chemical

interactions between oocyst wall macromolecules and the glass-bead collector. Using AFM studies, Considine et al. (60, 61) examined the interaction between *C. parvum* oocysts and silica surfaces similar to those used here. Their results were in qualitative agreement with measurements made in AFM studies using different tip-sample systems where the observed behavior was attributed to molecular bridging by macromolecules (62–65). Considine et al. (60, 61) propose that once the silica and oocyst surfaces contact each other, protein-linked tethering could occur. In fact, these authors suggest that protein molecules could readily bridge oocyst and glass surfaces several tens of nanometers out from hard-wall contact (e.g., where the oocyst is held in a secondary energy well) (61). Such specific interfacial protein interactions between the oocyst wall and glass-bead collectors could explain the reduced degree of particle release observed in the *C. parvum* elution experiment.

It is also interesting to note the different shapes of the elution peaks in Figures 7a and b. In the experiment conducted with latex particles (Figure 7b), the first elution peak (obtained after injection of 1 mM KHCO_3) is tall and narrow, whereas the second peak (obtained after injection of 1 mM KOH) is relatively insignificant. In comparison, with *C. parvum* oocysts, the two elution peaks have a short, broad shape and are more evenly distributed (Figure 7a). This difference in microsphere and oocyst release behavior could be related to the governing attachment mechanisms in each system. Elimination of the secondary energy well (following a sharp decrease in solution ionic strength) results in rapid release of retained microspheres (Figure 7b). On the other hand, a similar change in solution conditions in an experiment conducted with *C. parvum* results in slow and incomplete release of oocysts (as noted earlier). This slower elution of oocysts in comparison to latex microspheres may be related to the proposed specific surface interactions between oocyst wall proteins and the glass-bead collector. Such protein-tethering could retard or even completely inhibit oocyst release.

Implications for Oocyst Transport in Subsurface Porous Media. Measurements of retained *Cryptosporidium parvum* oocyst concentration were found to be in considerable disagreement with predictions of oocyst transport based on classical colloid filtration theory. These results have important implications with respect to predictions of oocyst removal in natural and engineered aquatic systems. In Figure 8, calculations of oocyst transport potential based on CFT (using the measured values of α_{BTC} in Table 1) are compared to calculations based on the DDM model (using the fitted parameter values in Table 2). The degree of oocyst removal is plotted as a function of travel distance for two cases: 1 mM and 10 mM ionic strength, in parts a and b, respectively, of Figure 8. The results shown in Figure 8 demonstrate how CFT significantly overestimates (by several orders of magnitude) predictions of oocyst removal in comparison to the DDM model. At the lowest ionic strength considered (Figure 8a), CFT predicts 5 log removal (i.e., $C/C_0 = 0.00001$) at a travel distance of 6 m, whereas calculations based on the DDM model suggest less than one log removal (i.e., $C/C_0 \approx 0.1$). This comparison reveals the potential risk when predictions of oocyst transport are assessed using CFT. In its Long-Term 2 Enhanced Surface Water Treatment Rule (LT2ESWTR), the U.S. EPA grants up to 1 log additional removal credit for *C. parvum* to water utilities using bank filtration wells located at least 15 m from the source (13). This design criterion is clearly in better accord with the DDM model than predictions based on CFT (Figure 8a). In fact, the calculations shown in Figure 8 suggest that the LT2ESWTR log credits are conservative relative to the DDM model. The better agreement observed between experimental results and the DDM model (Figure 6) and the comparison shown in

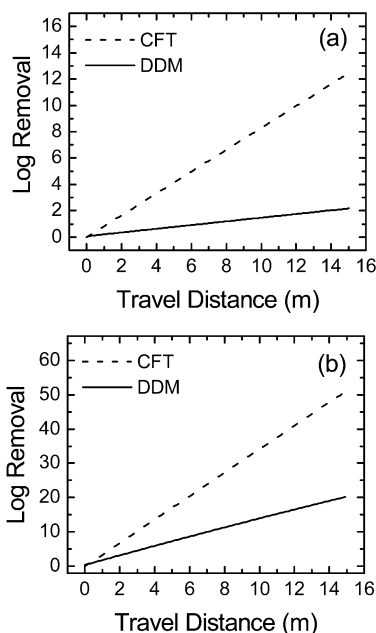


FIGURE 8. Predictions of oocyst log removal based on the proposed DDM model (solid lines) and the classical CFT (dashed lines) plotted as a function of travel distance for two different ionic strengths: (a) 1 mM and (b) 10 mM. CFT parameters were calculated values of α_{BTC} from Table 1, and DDM model parameters were fitted values from Table 2.

Figure 8 emphasize the shortcomings of CFT and the importance of considering improved particle transport models such as the proposed DDM approach.

It should be noted that the experiments described in this paper were conducted under well-controlled laboratory conditions using simple (1:1) electrolyte solutions and uniform, spherical glass-bead collectors. However, in subsurface environments, such as those typical of bank filtration sites, various factors not accounted for in these experiments influence the degree of microbe removal. For instance, the occurrence of iron oxide coatings on subsurface solid matrix may increase oocyst deposition (18, 59), whereas the presence of natural organic matter (NOM) may enhance oocyst transport (59, 66). Physical straining of oocysts is also expected to play an important role in such settings (15, 67, 68). Because CFT is based on the assumption of a single, constant microbe deposition rate, it is clearly ill-posed to describe such a problem. While the DDM model may not account for these mechanisms implicitly, the consideration of simultaneous “fast” and “slow” deposition allows for inclusion of factors such as iron oxide coatings and the stabilizing effect of NOM.

Acknowledgments

The authors acknowledge the support of the U.S. Environmental Protection Agency (Award CR-82901001-0), the U.S. Department of Agriculture (Award 2002-35102-12600), and the Natural Sciences and Engineering Research Council of Canada (NSERC) for a graduate student fellowship to N.T. The authors also thank W. P. Johnson for sharing the packed bed extrusion technique.

Literature Cited

- (1) *Emerging infections: microbial threats to health in the United States*; Lederberg, J., Shope, R. E., Oaks, S. C. J., Eds.; National Academy Press: Washington, DC, 1992.
- (2) Rose, J. B. Environmental ecology of *Cryptosporidium* and public health implications. *Annu. Rev. Public Health* **1997**, *18*, 135–161.
- (3) Smith, H. V. *Cryptosporidium* and Water – a Review. *J. Inst. Water Environ. Manage.* **1992**, *6*, 443–451.

- (4) Mawdsley, J. L.; Bardgett, R. D.; Merry, R. J.; Pain, B. F.; Theodorou, M. K. Pathogens in Livestock Waste, Their Potential for Movement through Soil and Environmental-Pollution. *Appl. Soil Ecol.* **1995**, *2*, 1–15.
- (5) Wolfson, J. S.; Richter, J. M.; Waldron, M. A.; Weber, D. J.; McCarthy, D. M.; Hopkins, C. C. *Cryptosporidiosis* in immunocompetent patients. *N. Engl. J. Med.* **1985**, *312*, 1278–1282.
- (6) Casemore, D. P.; Wright, S. E.; Coop, R. L. In *Cryptosporidium and Cryptosporidiosis*; Fayer, R., Ed.; CRC Press: Boca Raton, FL, 1997; pp 65–92.
- (7) Lisle, J. T.; Rose, J. B. *Cryptosporidium* Contamination of Water in the USA and UK – a Minireview. *J. Water Supply Res. Technol.-Aqua* **1995**, *44*, 103–117.
- (8) Smith, H. V.; Rose, J. B. Waterborne *cryptosporidiosis*: Current status. *Parasitol. Today* **1998**, *14*, 14–22.
- (9) West, P. A. Human pathogenic viruses and parasites: emerging pathogens in the water cycle. *J. Appl. Bacteriol. Suppl.* **1991**, *70*, 107S–114S.
- (10) Campbell, I.; Tzipori, A. S.; Hutchison, G.; Angus, K. W. Effect of disinfectants on survival of *Cryptosporidium* oocysts. *Vet. Rec.* **1982**, *111*, 414–415.
- (11) Hayes, E. B.; Matte, T. D.; O'Brien, T. R.; McKinley, T. W.; Logsdon, G. S.; Rose, J. B.; Ungar, B. L. P.; Word, D. M.; Pinsky, P. F.; Cummings, M. L.; Wilson, M. A.; Long, E. G.; Hurwitz, E. S.; Juranek, D. D. Large community outbreak of *cryptosporidiosis* due to contamination of a filtered public water supply. *N. Engl. J. Med.* **1989**, *320*, 1372–1376.
- (12) Timms, S.; Slade, J. S.; Fricker, C. R. Removal of *Cryptosporidium* by Slow Sand Filtration. *Water Sci. Technol.* **1995**, *31*, 81–84.
- (13) Tufenkji, N.; Ryan, J. N.; Elimelech, M. The promise of bank filtration. *Environ. Sci. Technol.* **2002**, *36*, 422a–428a.
- (14) Huck, P. M.; Coffey, B. M.; Emelko, M. B.; Maurizio, D. D.; Slawson, R. M.; Anderson, W. B.; van den Oever, J.; Douglas, I. P.; O'Melia, C. R. Effects of filter operation on *Cryptosporidium* removal. *J. Am. Water Works Assoc.* **2002**, *94*, 97–111.
- (15) Tufenkji, N.; Miller, G. F.; Ryan, J. N.; Harvey, R. W.; Elimelech, M. Transport of *Cryptosporidium* Oocysts in Porous Media: Role of Straining and Physicochemical Filtration. *Environ. Sci. Technol.* **2004**, *38*, 5932–5938.
- (16) Roy, S. B.; Dzombak, D. A. Colloid release and transport processes in natural and model porous media. *Colloid Surf. A: Physicochem. Eng. Asp.* **1996**, *107*, 245–262.
- (17) Harmand, B.; Rodier, E.; Sardin, M.; Dodds, J. Transport and capture of submicron particles in a natural sand: short column experiments and a linear model. *Colloid Surf. A: Physicochem. Eng. Asp.* **1996**, *107*, 233–244.
- (18) Elimelech, M.; Nagai, M.; Ko, C. H.; Ryan, J. N. Relative insignificance of mineral grain zeta potential to colloid transport in geochemically heterogeneous porous media. *Environ. Sci. Technol.* **2000**, *34*, 2143–2148.
- (19) Bai, R.; Tien, C. Particle Deposition under Unfavorable Surface Interactions. *J. Colloid Interface Sci.* **1999**, *218*, 488–499.
- (20) Franchi, A.; O'Melia, C. R. Effects of Natural Organic Matter and Solution Chemistry on the Deposition and Reentrainment of Colloids in Porous Media. *Environ. Sci. Technol.* **2003**, *37*, 1122–1129.
- (21) McDowell-Boyer, L. M. Chemical Mobilization of Micron-Sized Particles in Saturated Porous Media under Steady Flow Conditions. *Environ. Sci. Technol.* **1992**, *26*, 586–593.
- (22) Tobiason, J. E. Ph.D. Dissertation, The Johns Hopkins University, 1987.
- (23) Elimelech, M. Effect of Particle-Size On the Kinetics of Particle Deposition Under Attractive Double-Layer Interactions. *J. Colloid Interface Sci.* **1994**, *164*, 190–199.
- (24) Elimelech, M.; O'Melia, C. R. Kinetics of Deposition of Colloidal Particles in Porous-Media. *Environ. Sci. Technol.* **1990**, *24*, 1528–1536.
- (25) Elimelech, M.; O'Melia, C. R. Effect of Particle-Size On Collision Efficiency in the Deposition of Brownian Particles With Electrostatic Energy Barriers. *Langmuir* **1990**, *6*, 1153–1163.
- (26) Hsu, B.-M.; Huang, C. P.; Pan, J. R. Filtration behaviors of *Giardia* and *Cryptosporidium* – Ionic strength and pH effects. *Water Res.* **2001**, *35*, 3777–3782.
- (27) Redman, J. A.; Walker, S. L.; Elimelech, M. Bacterial adhesion and transport in porous media: role of the secondary energy minimum. *Environ. Sci. Technol.* **2004**, *38*, 1777–1785.
- (28) Harvey, R. W.; Garabedian, S. P. Use of Colloid Filtration Theory in Modeling Movement of Bacteria through a Contaminated Sandy Aquifer. *Environ. Sci. Technol.* **1991**, *25*, 178–185.
- (29) Tufenkji, N.; Elimelech, M. Breakdown of Colloid Filtration Theory: Role of Secondary Energy Minimum and Surface Charge Heterogeneities. *Langmuir* **2005**, *21*, 841–852.

- (30) Tufenkji, N.; Redman, J. A.; Elimelech, M. Interpreting deposition patterns of microbial particles in laboratory-scale column experiments. *Environ. Sci. Technol.* **2003**, *37*, 616–623.
- (31) Tufenkji, N.; Elimelech, M. Deviation from the Classical Colloid Filtration Theory in the Presence of Repulsive DLVO Interactions. *Langmuir* **2004**, *20*, 10818–10828.
- (32) Albinger, O.; Biesemeyer, B. K.; Arnold, R. G.; Logan, B. E. Effect of Bacterial Heterogeneity on Adhesion to Uniform Collectors by Monoclonal Populations. *FEMS Microbiol. Lett.* **1994**, *124*, 321–326.
- (33) Baygents, J. C.; Glynn, J. R.; Albinger, O.; Biesemeyer, B. K.; Ogden, K. L.; Arnold, R. G. Variation of surface charge density in monoclonal bacterial populations: Implications for transport through porous media. *Environ. Sci. Technol.* **1998**, *32*, 1596–1603.
- (34) Bolster, C. H.; Mills, A. L.; Hornberger, G. M.; Herman, J. S. Spatial distribution of deposited bacteria following miscible displacement experiments in intact cores. *Water Resour. Res.* **1999**, *35*, 1797–1807.
- (35) Camesano, T. A.; Logan, B. E. Influence of Fluid Velocity and Cell Concentration on the Transport of Motile and Nonmotile Bacteria in Porous Media. *Environ. Sci. Technol.* **1998**, *32*, 1699–1708.
- (36) Martin, M. J.; Logan, B. E.; Johnson, W. P.; Jewett, D. G.; Arnold, R. G. Scaling bacterial filtration rates in different sized porous media. *J. Environ. Eng.-ASCE* **1996**, *122*, 407–415.
- (37) Redman, J. A.; Estes, M. K.; Grant, S. B. Resolving macroscale and microscale heterogeneity in virus filtration. *Colloid Surf. A: Physicochem. Eng. Asp.* **2001**, *191*, 57–70.
- (38) Yao, K. M.; Habibian, M. T.; O'Melia, C. R. Water and Wastewater Filtration – Concepts and Applications. *Environ. Sci. Technol.* **1971**, *5*, 1105–1112.
- (39) Li, X.; Scheibe, T. D.; Johnson, W. P. Apparent Decreases in Colloid Deposition Rate Coefficients with Distance of Transport under Unfavorable Deposition Conditions: A General Phenomenon. *Environ. Sci. Technol.* **2004**, *38*, 5616–5625.
- (40) Harter, T.; Wagner, S.; Atwill, E. R. Colloid transport and filtration of *Cryptosporidium parvum* in sandy soils and aquifer sediments. *Environ. Sci. Technol.* **2000**, *34*, 62–70.
- (41) Mawdsley, J. L.; Brooks, A. E.; Merry, R. J. Movement of the protozoan pathogen *Cryptosporidium parvum* through three contrasting soil types. *Biol. Fertil. Soils* **1996**, *21*, 30–36.
- (42) Hunter, R. J. *Foundations of Colloid Science*; Oxford University Press: New York, 2001.
- (43) Grolimund, D.; Elimelech, M.; Borkovec, M.; Barmettler, K.; Kretzschmar, R.; Sticher, H. Transport of in situ mobilized colloidal particles in packed soil columns. *Environ. Sci. Technol.* **1998**, *32*, 3562–3569.
- (44) Tufenkji, N.; Elimelech, M. Correlation Equation for Predicting Single-Collector Efficiency in Physicochemical Filtration in Saturated Porous Media. *Environ. Sci. Technol.* **2004**, *38*, 529–536.
- (45) Dai, X.; Hozalski, R. M. Evaluation of Microspheres as Surrogates for *Cryptosporidium parvum* Oocysts in Filtration Experiments. *Environ. Sci. Technol.* **2003**, *37*, 1037–1042.
- (46) Brush, C. F.; Walter, M. F.; Anguish, L. J.; Ghiorse, W. C. Influence of Pretreatment and Experimental Conditions on Electrophoretic Mobility and Hydrophobicity of *Cryptosporidium parvum* Oocysts. *Appl. Environ. Microbiol.* **1998**, *64*, 4439–4445.
- (47) Considine, R. F.; Dixon, D. R.; Drummond, C. J. Oocysts of *Cryptosporidium parvum* and model sand surfaces in aqueous solutions: an atomic force microscope (AFM) study. *Water Res.* **2002**, *36*, 3421–3428.
- (48) Derjaguin, B. V.; Landau, L. D. Theory of the stability of strongly charged lyophobic sols and of the adhesion of strongly charged particles in solutions of electrolytes. *Acta Physicochim. URSS* **1941**, *14*, 733–762.
- (49) Verwey, E. J. W.; Overbeek, J. T. G. *Theory of the Stability of Lyophobic Colloids*; Elsevier: Amsterdam, 1948.
- (50) Simoni, S. F.; Bosma, T. N. P.; Harms, H.; Zehnder, A. J. B. Bivalent Cations Increase Both the Subpopulation of Adhering Bacteria and Their Adhesion Efficiency in Sand Columns. *Environ. Sci. Technol.* **2000**, *34*.
- (51) Medema, G. J.; Schets, F. M.; Teunis, P. F. M.; Havelaar, A. H. Sedimentation of Free and Attached *Cryptosporidium* Oocysts and *Giardia* Cysts in Water. *Appl. Environ. Microbiol.* **1998**, *64*, 4460–4466.
- (52) Tobiasson, J. E.; O'Melia, C. R. Physicochemical aspects of particle removal in depth filtration. *J. Am. Water Works Assoc.* **1988**, *80*, 54–64.
- (53) Hogg, R.; Healy, T. W.; Fuerstenau, D. W. Mutual coagulation of colloidal dispersions. *Trans. Faraday Soc.* **1966**, *62*, 1638–1651.
- (54) Gregory, J. Approximate expression for retarded van der Waals interaction. *J. Colloid Interface Sci.* **1981**, *83*, 138–145.
- (55) Hahn, M. W.; O'Melia, C. R. Deposition and Reentrainment of Brownian Particles in Porous Media under Unfavorable Chemical Conditions: Some Concepts and Applications. *Environ. Sci. Technol.* **2004**, *38*, 210–220.
- (56) Litton, G. M.; Olson, T. M. Particle size effects on colloid deposition kinetics: evidence of secondary minimum deposition. *Colloid Surf. A: Physicochem. Eng. Asp.* **1996**, *107*, 273–283.
- (57) Redman, J. A.; Grant, S. B.; Olson, T. M.; Estes, M. K. Pathogen filtration, heterogeneity, and the potable reuse of wastewater. *Environ. Sci. Technol.* **2001**, *35*, 1798–1805.
- (58) Hahn, M. W.; Abadzic, D.; O'Melia, C. R. Aquasols: On the Role of Secondary Minima. *Environ. Sci. Technol.* **2004**, *38*, 5915–5924.
- (59) Ryan, J. N.; Elimelech, M. Colloid mobilization and transport in groundwater. *Colloid Surf. A* **1996**, *107*, 1–56.
- (60) Considine, R. F.; Drummond, C. J.; Dixon, D. R. Force of Interaction between a Biocolloid and an Inorganic Oxide: Complexity of Surface Deformation, Roughness, and Brushlike Behavior. *Langmuir* **2001**, *17*, 6325–6335.
- (61) Considine, R. F.; Dixon, D. R.; Drummond, C. J. Laterally-Resolved Force Microscopy of Biological Microspheres – Oocysts of *Cryptosporidium Parvum*. *Langmuir* **2000**, *16*, 1323–1330.
- (62) Dammer, U.; Popescu, O.; Wagner, P.; Anselmetti, D.; Guntherodt, H.-J.; Misevic, G. N. Binding strength between cell-adhesion proteoglycans measured by atomic force microscopy. *Science* **1995**, *267*, 1173–1175.
- (63) Chen, X.; Davies, M. C.; Roberts, C. J.; Tendler, S. J. B.; Williams, P. M. Recognition of Protein Adsorption onto Polymer Surfaces by Scanning Force Microscopy and Probe-Surface Adhesion Measurements with Protein-Coated Probes. *Langmuir* **1997**, *13*, 4106–4111.
- (64) Ortiz, C.; Hadziioannou, G. Entropic Elasticity of Single Polymer Chains of Poly(methacrylic acid) Measured by Atomic Force Microscopy. *Macromolecules* **1999**, *32*, 780–787.
- (65) Stuart, J. K.; Hlady, V. Effects of Discrete Protein-Surface Interactions in Scanning Force Microscopy Adhesion Force Measurements. *Langmuir* **1995**, *11*, 1368–1374.
- (66) Dai, X.; Hozalski, R. M. Effect of NOM and biofilm on the removal of *Cryptosporidium parvum* oocysts in rapid filters. *Water Res.* **2002**, *36*, 3523–3532.
- (67) Poppen, J. W. A.; Mporokoso, A.; Schijven, J. F. Determining straining of *Escherichia coli* from breakthrough curves. *J. Contam. Hydrol.* **2005**, *76*, 191–210.
- (68) Bradford, S. A.; Yates, S. R.; Bettahar, M.; Simunek, J. Physical factors affecting the transport and fate of colloids in saturated porous media. *Water Resour. Res.* **2002**, *38*, 1327–1338.

Received for review November 1, 2004. Revised manuscript received March 14, 2005. Accepted March 15, 2005.

ES048289Y